DYNAMIC RESPONSE, BUCKLING AND COLLAPSING OF ELASTIC-PLASTIC STRAIGHT COLUMNS UNDER AXIAL SOLID-FLUID SLAMMING COMPRESSION—I. EXPERIMENTS

Qingjie Zhang,† Shiqi Li and Jijia Zheng

Department of Naval Architecture and Ocean Engineering, Huazhong University of Science and Technology, 430074, Wuhan, P.R.C.

Abstract—The dynamic behavior of straight elasto–plastic columns subjected to axial solid–fluid slamming compression is investigated experimentally in the present study. Two classes of columns are tested: large slenderness columns with the static Euler strain ε_{crE} smaller than the yield strain ε_y, and middle slenderness ones with the ε_{crE} close to the ε_y. Three critical conditions for each of the columns are observed from the experiments: plastic incipience, buckling, and plastic collapse. These conditions are defined by introducing three critical loading strains: plastic, buckling, and collapse axial loading strains. The three critical strain values for each tested column are reported in the paper. The results indicate that: (1) the plasticity in a column appears first at the center and the plastic region is always at the middle length; (2) according to the buckling definition, the type 1 columns buckle elastically while the type 2 buckle plastically; (3) the column's load-carrying capacity is insensitive to the elasto-plastic loading histories (sequences) which the structure experiences before the plastic collapse occurs and is essentially governed by the dynamic post-buckling elasto-plastic behavior in one slamming; and (4) at the critical buckling loading magnitudes the column's response becomes dominated by motion in the fundamental mode.

NOTATION

ε_c	peak axial loading strain
$\varepsilon_1, \varepsilon_2$	resultant strains at the column's two sides
ε_b	bending strain, $\varepsilon_b = (\varepsilon_1 - \varepsilon_2)/2$
$|\varepsilon_b|_{max}$	maximum bending strain
$|\varepsilon|_{max}$	maximum resultant strain
$\varepsilon_{c,crb}$	critical buckling axial loading strain
$\varepsilon_{c,cry}$	critical plastic axial loading strain
$\varepsilon_{c,crf}$	critical collapse axial loading strain
$\varepsilon_{1r}, \varepsilon_{2r}$	residual strains at the column's two sides
ε_{crE}	static Euler critical strain of clamped columns, $\varepsilon_{crE} = (\pi/\lambda_{eff})^2$
t_0	slamming duration
t_p	peak slamming time
t_M	maximum response time
t_s	response cease time
w_0	maximum initial geometric imperfection
H	slamming height
E	elastic module
ε_y	yield strain of the column's material
ρ	density of the column's material
L	effective length of the specimen
b, h	width and thickness of specimen's cross-section
λ_{eff}	slenderness of clamped columns, $\lambda_{eff} = (\sqrt{3}L)/h$
C_0	compressive stress wave speed.

INTRODUCTION

Buckling phenomena may be divided into two classes for axial dynamically loaded columns: parametric resonance, with loading of an axial periodic compression, and buckling in which the structures are subjected to axial sudden loads. The parameter resonance is also called vibration buckling (Lindberg and Florence, 1987), which was well discussed by Bolotin (1964). For this kind of buckling, the column's condition is identified as being critical if the parametric combination among the structure and load falls into the stable and unstable region boundaries in the parameter space. The unstable condition for the para-

metric resonance is characterized by the column's unbounded response or escaping motion.

The problem of suddenly loaded columns can be subdivided into pulse buckling with respect to impulsive load, and step-loading in which the structures are acted upon by step loads with infinite duration and constant magnitude. Pulse buckling of columns was first considered by Taub and Kong (1934) and has since been extended by many researchers. Based on different assumptions for the boundary condition at the column's impact end, three analysis models are employed: (a) an axial load problem (Housner and Tso, 1962; Abrahamson and Goodier, 1966; Lindberg, 1965; Taub and Kong, 1934); (b) a constant velocity problem (Lee, 1981); and (c) a constant mass problem (Ari-Gur *et al.*, 1982; Kunistomo *et al.*, 1985; Koji, 1986, 1987; Grybos, 1973; Hayashi and Sano, 1972, 1973). In experiments, studies on the subject are primarily concentrated on the third model. The pulse buckling problem is one of a "dynamic response" type rather than an "escaping motion" type of instability (Simitses, 1987). According to this, it can be said that the condition is critical if the structure reaches (but does not exceed) some allowable kinematic status.

For the step-load case, Reiss and Matkowsky (1971) treated the nonlinear dynamic buckling of elastic columns and Jonse and Dos Reis (1980) examined the dynamic buckling of elastic–plastic columns. These studies indicate that the columns exhibit an "escaping motion" type of dynamic instability. Actually, this extreme case is an idealized treatment for suddenly loaded columns in practice.

The pulse buckling phenomenon is usually encountered in solid–solid impact situations in which the loading pulse has strong magnitude and microsecond-range duration. When columns are subjected to this kind of solid–solid impact, due to the microsecond-range duration, the response growth stemming from initial imperfections after impact is important while the plastic failure is not appreciable.

Also, for suddenly-loaded columns, there is another kind of buckling phenomenon which is related to fluid–structure slamming. The phenomenon may be encountered in many fields, such as ship slamming, landing of flying boats, etc. This problem is characterized by load–time histories in the millisecond range. Because of the millisecond-range duration, compression–bending coupling under large slamming values may impel slammed columns into sufficiently large deformation that plastic collapse is possible. This makes apparent that the columns may show several different critical conditions during slamming, which cannot be interpreted by vibration buckling, pulse or step-load buckling. The present study is to explore experimentally the dynamic buckling behavior of elastic–plastic columns undergoing fluid–structure slamming compression and to trace the critical conditions.

Results from experiments on 15 clamped–clamped columns, with the lengths from 400 to 600 mm, are reported in the present paper. For each column, three critical conditions are observed in the experiments; plastic incipience, buckling and plastic collapse. These conditions are estimated by introducing three critical loading strains which are defined as follows:

$\varepsilon_{c,crb}$: the critical buckling peak axial loading strain at which the maximum bending strain, near the center of the column, grows to a value equal to the axial loading strain.

$\varepsilon_{c,cry}$: the critical plastic peak axial loading strain at which the maximum compressive bending resultant strain grows to a value equal to the yield strain of the material.

$\varepsilon_{c,crf}$: the critical collapse peak axial loading strain beyond which further increases in drop height result in decreases in peak loading strain rather than increases.

For each column, the three critical loading magnitudes are reported. The data and definitions from the present experiments provide a basic understanding of the slammed columns.

TEST SET-UP AND PROCEDURE

The test rig simulating the buckling phenomenon of columns subjected to an axial fluid–structure slamming compression is shown in Fig. 1, which consists of seven principal parts: (1) electric motor; (2) 6m-high slamming tower; (3) sliding vehicle guides; (4) electric–magnetic releaser; (5) 450 kg weight sliding vehicle, where the upper part is hooked by the releaser and can move up and down along its guides; (6) 500 kg weight axial loading
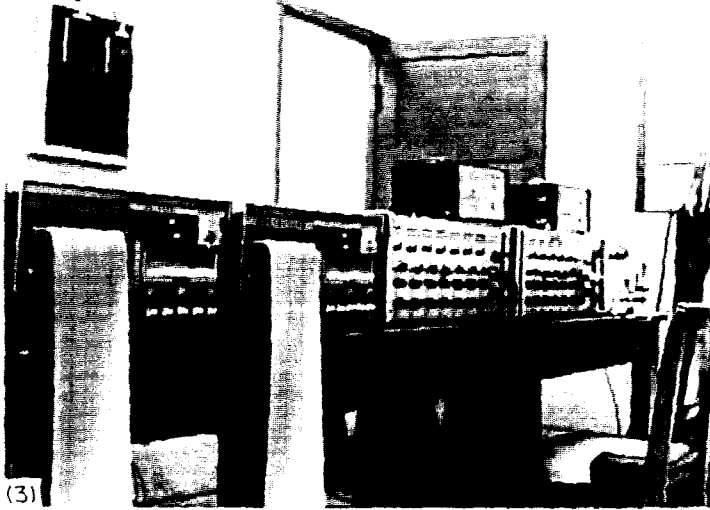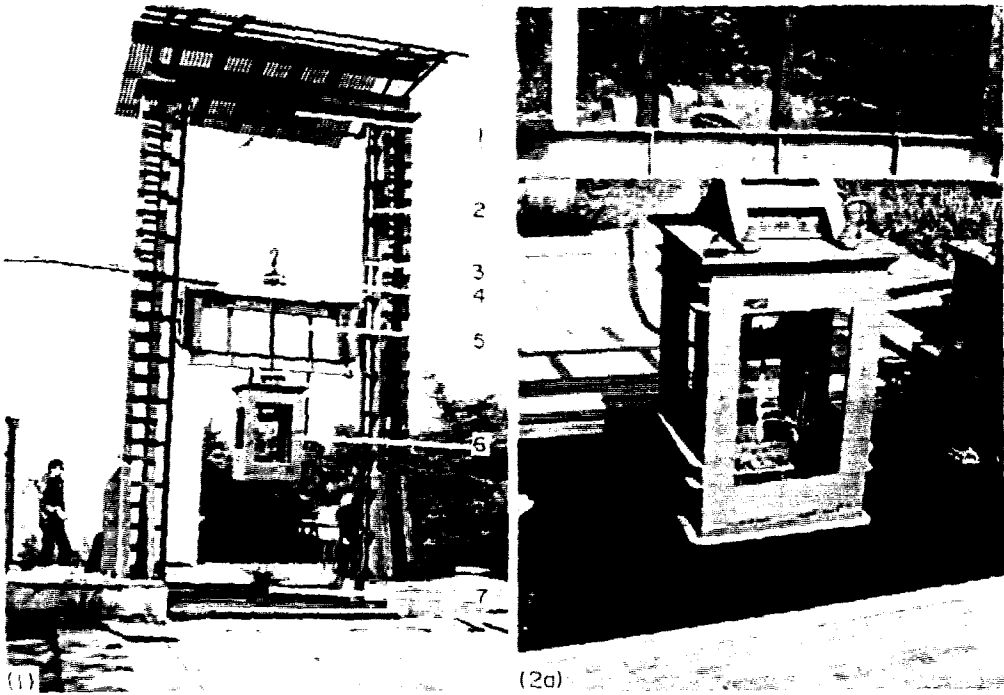
Fig. 1. Test set-up for slamming buckling. 1, electric motor; 2, slamming tower; 3, sliding vehicle guides; 4, releaser; 5, sliding vehicle; 6, axial loading device; 7, water pool.

Fig. 2(a). Axial loading device (see also Fig. 2(b)).
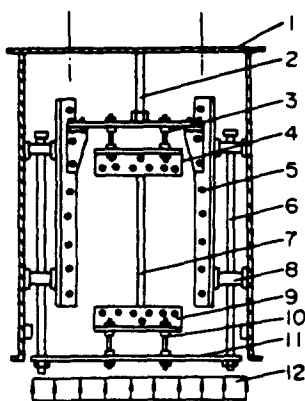
Fig. 3. Dynamic signals recording system.

Fig. 2(b). Axial loading device. (1) outer casing; (2) reinforcement support; (3) upper sensors; (4) upper boundary; (5) flank boundary; (6) guiding rods; (7) specimen; (8) sliding guides; (9) lower boundary; (10) lower sensors; (11) bottom plate; (12) slamming load.

device attached to the lower part of the sliding vehicle; and (7) 4m-deep water pool. In experiments, the electric–magnetic releaser is automatically controlled such that the recording of signals to be measured keeps the same time as the releasing of the axial loading device.

The axial loading device is indicated in the enlarged detail in Fig. 2. It has a rigid bottom plate which can move up when subjected to slamming. The movement of the plate is governed by its sliding guides and strictly restrained to the vertical direction. When the axial loading device is suddenly released from a certain height and falls down to the water surface, slamming happens between the plate and the water surface, and the slamming load is immediately applied axially to the specimen.

The recording system of dynamic signals is shown in Fig. 3. In experiments, the strain signals of a specimen to be measured are transmitted to the two YD-15 type dynamic strain gages through the remote-measurement cables, and recorded by the four SC-16 light wave form recorders. In order to trace the critical conditions, a specimen is repeatedly loaded through adjusting different slamming heights. The initial slamming height is low and then increased gradually until plastic collapse takes place.

Three kinds of boundary conditions for columns can be carried out through the axial loading device. They are: (a) clamped supporting boundary; (b) simply supporting boundary, and (c) simply clamped supporting boundary. The first two kinds of boundaries are indicated in Fig. 4. For the present study, only the clamped condition is considered.

SPECIMEN CLASSIFICATION

The rectangular cross-section specimens and clamped boundary condition are considered in experiments as shown in Fig. 5. The specimen sizes, effective slenderness and
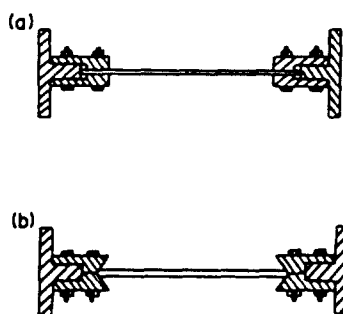
(a)

(b)

Fig. 4. Column boundary conditions. (a) Clamped supporting boundary; (b) simply supporting boundary.

Table 1. Clamped steel columns under axial slamming

Specimen no.	L (mm)	b (mm)	h (mm)	λ_{eff}	ε_{crE} ($\mu\varepsilon$)	$\varepsilon_{c,rb}$ (μc)	$\varepsilon_{c,cry}$ ($\mu\varepsilon$)	$\varepsilon_{c,crf}$ ($\mu\varepsilon$)	w_0 (mm)
S11	600.0	14.7	7.7	135.9	534.8	470.0	580.0	680.0	0.30
S12	600.0	14.6	7.7	135.7	536.2	480.0	600.0	680.0	0.35
S13	600.0	14.7	7.6	136.0	533.5	480.0	580.0	650.0	1.50
S14	600.0	14.7	7.7	135.7	536.2	470.0	560.0	660.0	1.05
S15	600.0	14.6	7.7	134.3	547.5	470.0	560.0	650.0	0.25
S21	500.0	14.2	7.7	112.5	780.2	540.0	600.0	800.0	0.30
S22	500.0	14.3	7.7	112.6	778.2	540.0	620.0	780.0	0.35
S23	500.0	14.4	7.7	112.8	776.2	550.0	640.0	790.0	1.00
S24	500.0	14.2	7.7	113.2	770.2	530.0	620.0	780.0	0.75
S25	500.0	14.3	7.7	112.0	786.2	550.0	610.0	760.0	1.00
S31	400.0	14.6	7.7	89.4	1234.9	820.0	750.0	900.0	0.25
S32	400.0	14.5	7.7	89.2	1241.3	820.0	750.0	910.0	0.45
S33	400.0	14.5	7.7	89.2	1241.3	850.0	760.0	930.0	0.75
S34	400.0	14.5	7.7	89.2	1241.3	840.0	760.0	920.0	0.45
S35	400.0	14.5	7.7	89.2	1241.3	840.0	750.0	920.0	1.20

static Euler strains are given in Table 1, in which the later experimental results for slamming cases are also listed for comparison. The real initial profiles of specimens in the thin direction of cross-section are measured, and the maximum initial geometric imperfections w_0 are also given in the table. The specimens are classified into two categories: (a) large slenderness columns (S11–S25), for which the static Euler strain ε_{crE} is smaller than the yield strain ε_y; and (b) middle slenderness columns (S31–S35), for which static Euler strain ε_{crE} is close to the ε_y. In addition, the material test is performed with five tensile samples; the stress–strain curve and the average properties are also presented in Fig. 5.

To determine the deformed profiles and plastic regions of the tested columns, several pairs of strain gages are arranged on both sides of a specimen. The gage arrangement of the type 1 columns is indicated in Fig. 5. For the type 2 columns, three pairs of gages are placed at points C, D and E, and one pair at A, near the impact end. It is noted that in
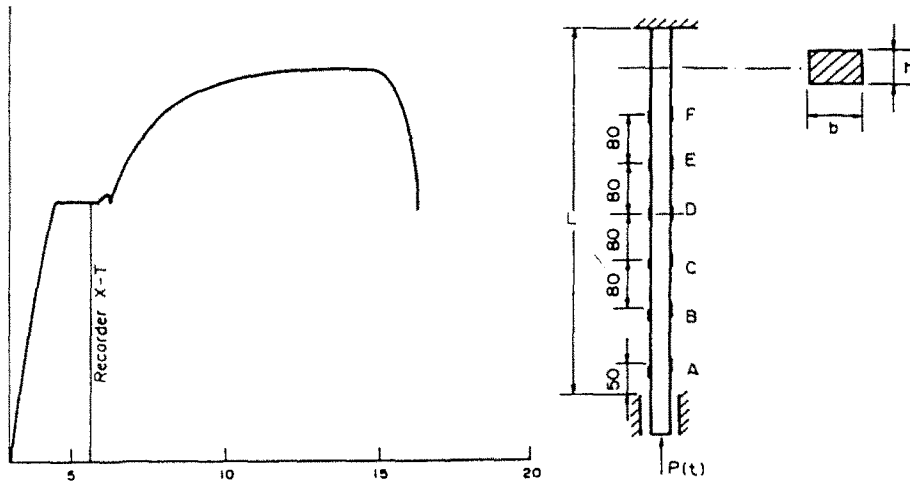
Sample No. 61
Area   161.50 mm^2
Elastic   22600. kg/mm^2

	Load (kg)	Elong. (mm)	Stress (kg/mm^2)	Strain (%)
YS	No data	No data	No data	No data
YP	4277.1	0.064697	26.469	0.12939
Max.	6365.5	46.800	39.393	93.600
Break	4236.9	58.500	26.220	117.00

Fig. 5. Material properties and gage arrangement. $\sigma_y = 2680$ kgf cm^{-2}; $\varepsilon_y = 1275$ $\mu\varepsilon$; $E = 2.102 \times 10^6$ kgf cm^{-2}; $\rho = 7.8 \times 10^3$ kg cm^{-3}; $C_0 = 5.19 \times 10^3$ m s^{-1}.
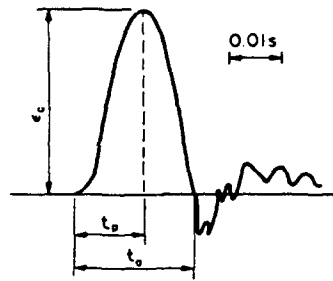
Fig. 6. A typical fluid–structure slamming pulse.

the present tests, the slamming load is measured by a pair of gages located at A rather than by the force sensors shown in Fig. 2.

RESULTS AND DISCUSSIONS

(1) *Slamming load and compressive motion*

A typical record for the slamming load is shown in Fig. 6, where ε_c, t_0 and t_p are the slamming peak value, duration and peak time, respectively. The test results for the two category specimens indicate that ε_c rises with increasing of slamming height and t_0 varies with the different slenderness ratio: the smaller the slenderness, the shorter the t_0. For a prescribed slenderness ratio, however, t_0 remains basically unchanged provided that the column does not collapse plastically.

t_0 ranges from 15 to 24 ms for the present two types of columns during elastic and elasto-plastic slamming without collapse appearance. At these durations, from 130 to 311 wave transits occur along the column length of 400 to 600 mm in the tests. This would make it apparent that there are no significant axial inertia effects. Table 2 indicates the compressive strain distribution of the type I columns. It also can be seen from the table that, except for the small experimental scatter, the strains are basically distributed uniformly along the length. Thus, it may be considered that the compressive motion is axially uniform.

(2) *Flexural vibration and bending mode*

Typical strain histories of the type I and type 2 columns under different slamming heights are presented in Figs 7 and 8, respectively. It is observed from the figures that the flexural vibration strongly depends on the slamming peak value ε_c. The motion is weak for small ε_c and becomes strong gradually with the load increase. When ε_c reaches a critical value $\varepsilon_{c,crb}$, a transition occurs at which the flexural vibration starts to become stronger than the compressive one. Before the transition, the compression–bending resultant response exhibits completely the compressive motion characters. After that, the response is divided into two phases: the first $(0 \leqslant t \leqslant t_0)$ and the second phase $(t_0 \leqslant t \leqslant t_s)$, where t_s is the response cease time. The former is called main response phase and the latter the secondary one. The main response is directly dependent on the slamming compression while the second is relevant to the maximum elastic bending strain energy stored in the first phase.

It is also observed from the two figures that the maximum resultant (bending plus compression) response appears later than the maximum compressive motion after the transition. This is more clear from Fig. 9 in which the development of the column's deformed profile is indicated with increasing load and time. Actually, Fig. 9 demonstrates that the

Table 2. Compressive strain distribution at t_p (specimen no. SI1, $t_p = 0.012$ s)

	A	B	C	D	E	F	
$H = 40$ mm	−325	−323	−367	−353	−363	−360	$\mu\varepsilon$
$H = 75$ mm	−600	−560	−567	−590	−600	−573	$\mu\varepsilon$
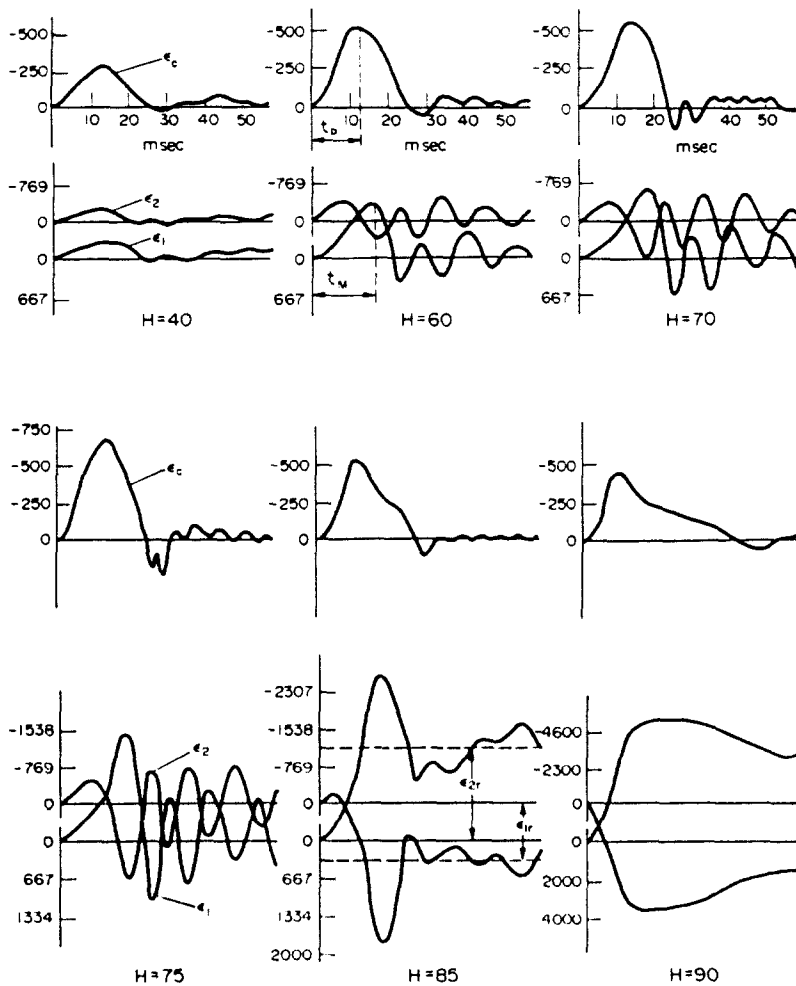
Fig. 7. Typical strain histories of type 1 columns (specimen no. S12). ε_c, axial loading strain near impact end ; ε_1, ε_2, resultant strains at center ($\mu\varepsilon$).

flexural response at t_p for the $H = 75$ mm drop height is smaller than that at t_M for the $H = 65$ mm, in which t_M is the maximum response time of the resultant strain. This indicates the important role of slamming duration in affecting the slammed columns' behavior when the columns are loaded by some critical magnitudes at which their response is dominated by the flexural vibration. Due to millisecond-range durations, the compressive–bending coupling under the critical slamming values cause the columns to undergo large deformation. Thus, plastic collapse of the structures is possible during slamming. This situation does not occur for columns subjected to solid–solid impact where response growth stemming from initial imperfections after impact while plastic failure is not appreciable because of the microsecond-range durations.

Figure 10 gives the S11 bending strain distributions along the length at the maximum response time t_M for different slamming heights. The results indicate that the bending strain for $H = 40$ mm has three zero values along the length while it has two for the greater drop heights. The phenomenon also occurs for the other tested type 1 columns. This means that the response mode shape of the type 1 columns is mode 2 for smaller slamming values while the response for greater loading magnitude is dominated by the fundamental one.

(3) *Plasticity and critical plastic condition*

In experiments, each specimen is loaded elastically and elasto-plastically until its plastic collapse takes place. A direct finding from the test results is that the axial compression is always elastic for all the slammed columns and thus plasticity only refers to the compressive–bending response.
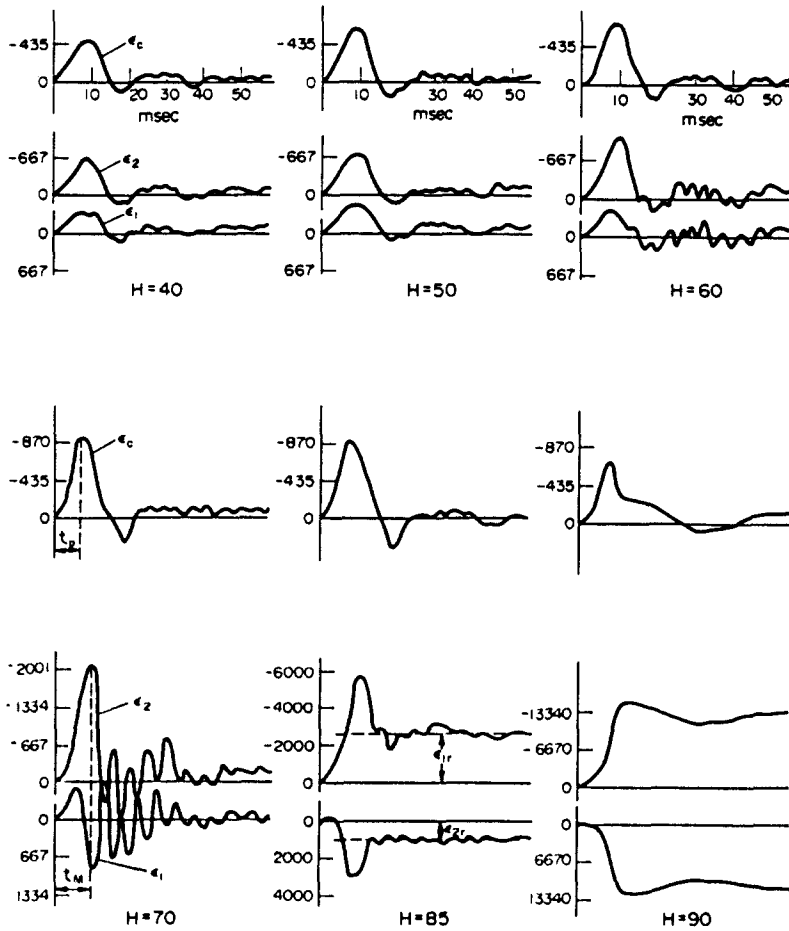
Fig. 8. Typical strain histories of type 2 columns (specimen no. S31). ε_c, axial loading strain near impact end ; ε_1, ε_2, resultant strains at center ($\mu\varepsilon$).
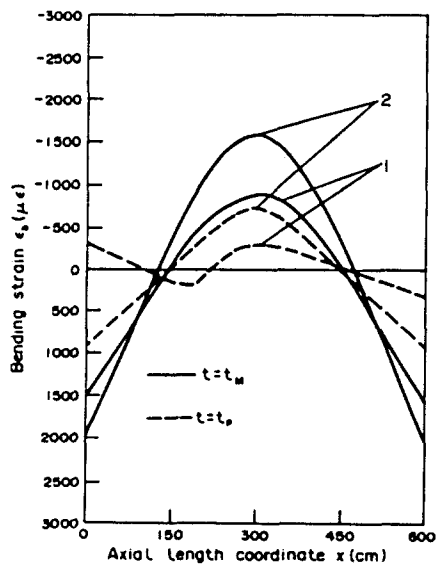
Fig. 9. Bending deformation comparison at t_p and t_M (specimen no. S11, $t_M = 0.016$ s). (1) $H = 65$, $\varepsilon_c > \varepsilon_{c,crh}$ (elastic) ; (2) $H = 75$ mm, $\varepsilon_c > \varepsilon_{c,crh}$ (plastic).
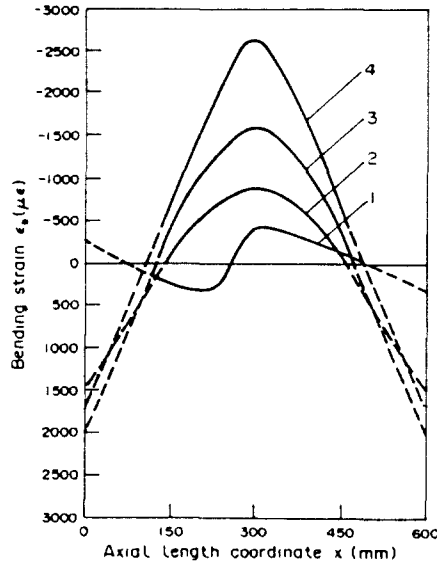
Fig. 10. Flexural response modes under different loading magnitudes ($t = t_M$, specimen no. S11).
(1) $H = 40$ mm; (2) $H = 65$ mm; (3) $H = 75$ mm; (4) $H = 85$ mm. Note: $\varepsilon_b \times 10$ versus x for $H = 40$.

It can be seen from Figs 7 and 8 that the elasto-plastic response for the different drop heights is divided into two phases: a quasi-elastic phase for the small loading magnitudes at which the columns still behave in an elastic way, and a plastic phase for the larger slamming values at which the residual strains remain in the response after impact.

To indicate the incipience and development of plasticity, the S11 elasto-plastic resultant strain distributions in two slamming tests are given in Table 3. It is observed from the table that plasticity appears first at the outer fibers of the central cross-section, then spreads along the length and thickness with time and load increase. However, the compressive and tensile plastic regions are always at the middle length.

Finally in this section, it is necessary to define a critical loading condition associated with plastic incipience for the present columns in order to divide the elastic and inelastic behavior. The condition is seen to occur for a column if its ε_c reaches (but does not exceed) a critical value $\varepsilon_{c,cry}$ at which the maximum resultant strain grows to a value equal to the yield strain of the material. $\varepsilon_{c,cry}$ is called the critical plastic axial loading strain.

(4) Buckling and plastic collapse

Conceptually, buckling of columns subjected to sudden and transient loads is related to characteristics of the dynamic response. For the present columns, we adapt by choosing the transition defined in Section 2 as the buckling kinematic status because the significant bending vibration appears and begins to become dominant at the transition. Thus, a

Table 3. Elasto-plastic resultant strain distribution (specimen no. S11)

		B	C	D (middle)	E	
$H = 75$ ($\varepsilon_c = 600$)	$t = t_p$	$\varepsilon_1 = -500$ $\varepsilon_2 = -600$	$\varepsilon_1 = -934$ $\varepsilon_2 = -200$	$\varepsilon_1 = -1334$ $\varepsilon_2 = 154$	$\varepsilon_1 = -1143$ $\varepsilon_2 = -296$	($\mu\varepsilon$)
	$t = t_M$	$\varepsilon_1 = -333$ $\varepsilon_2 = -233$	$\varepsilon_1 = -1401$ $\varepsilon_2 = 867$	$\varepsilon_1 = -1868$ $\varepsilon_2 = 1308$	$\varepsilon_1 = -1428$ $\varepsilon_2 = 815$	($\mu\varepsilon$)
$H = 85$ ($\varepsilon_c = 680$)	$t = t_p$	$\varepsilon_1 = -666$ $\varepsilon_2 = -567$	$\varepsilon_1 = -1600$ $\varepsilon_2 = -267$	$\varepsilon_1 = -1868$ $\varepsilon_2 = 615$	$\varepsilon_1 = -1244$ $\varepsilon_2 = -185$	($\mu\varepsilon$)
	$t = t_M$	$\varepsilon_1 = -583$ $\varepsilon_2 = 200$	$\varepsilon_1 = -1867$ $\varepsilon_2 = 1601$	$\varepsilon_1 = -2668$ $\varepsilon_2 = 2615$	$\varepsilon_1 = -1785$ $\varepsilon_2 = 1481$	($\mu\varepsilon$)

proposed criterion is : a column is identified as buckling if its ε_c reaches a critical value $\varepsilon_{c,crb}$ at which the maximum bending strain grows to a value equal to the axial loading magnitude. $\varepsilon_{c,crb}$ is called the critical buckling peak axial loading strain.

According to the buckling definition, it is clear that the buckling of an axially slammed column does not mean the loss of its load-carrying capacity. Actually, the load-carrying capacity loss is correlated to the plastic collapse. This is apparent from Figs 7 and 8, in which the columns cannot resist slamming when the drop height reaches $H = 85$ mm for S12 and at $H = 90$ mm for S31. In order to estimate the load-carrying capacity of the tested columns, we must give a definition for the critical condition associated with the load-carrying capacity loss. It is known from the results for the two types of columns that the loading duration of a column bears little change before the plastic collapse occurs. Based on the response characteristic and the fact that the maximum compressive–bending response always occurs within loading duration, the following definition may be introduced to estimate the load-carrying capacity : the column's loading is considered to be critical for plastic collapse if the peak axial loading strain ε_c reaches a critical value $\varepsilon_{c,crf}$ beyond which further increases in drop height result in decreases in peak loading strain rather than increases. $\varepsilon_{c,crf}$ is called critical collapse peak axial loading strain.

So far, three critical conditions for the present columns have been defined by introducing the three critical peak axial loading strains, which are plastic incipience, buckling and plastic collapse. In order to determine the critical strain values of the tested columns, the curves of maximum flexural strain $|\varepsilon_b|_{max}$ versus peak axial loading strain $|\varepsilon_c|$ and maximum resultant strain$|\varepsilon|_{max}$ versus $|\varepsilon_c|$ are plotted for each specimen. The two curves for S12, S21 and S31 are shown in Fig. 11. From the definition for the three critical conditions and the curves in Fig. 11, the three critical loading values of S12, S21 and S31
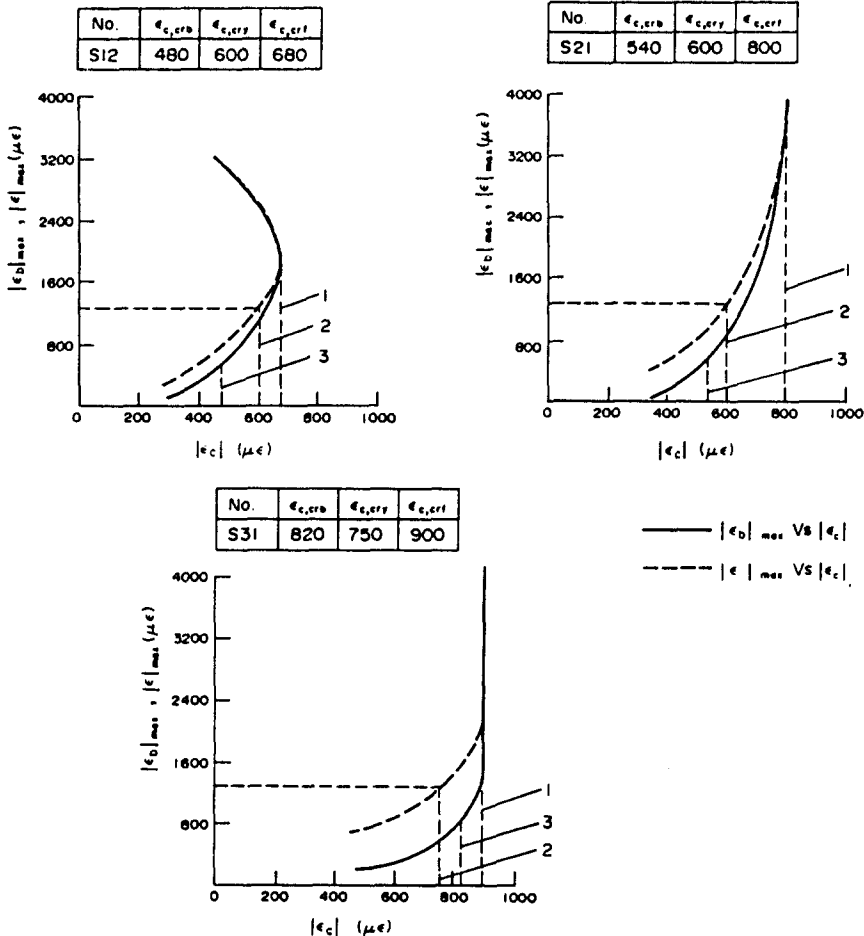

Fig. 11. Determination of critical axial loading strains. (1) $\varepsilon_{c,crf}$; (2) $\varepsilon_{c,cry}$; (3) $\varepsilon_{c,crb}$.
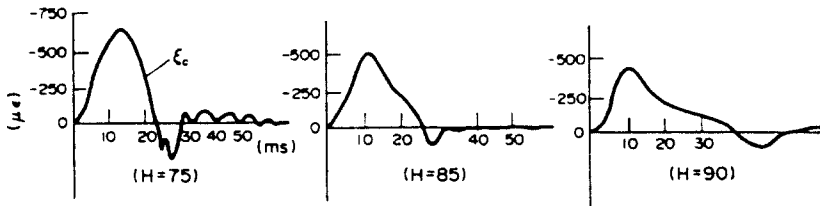
Fig. 12. Loading pulse shapes at and beyond $\varepsilon_{c,crf}$ slamming.

are obtained. For the other specimens, their characteristic curves are similar to those in Fig. 11 and the respective critical values have been given in Table 1.

From Fig. 11 and Table 1, it is easily found that the relationship $\varepsilon_{c,crb} < \varepsilon_{c,cry} < \varepsilon_{c,crf}$ is valid for the type 1 columns while the inequality $\varepsilon_{c,cry} < \varepsilon_{c,crb} < \varepsilon_{c,crf}$ holds true for the type 2 columns. This means that the first category columns buckle elastically and the second plastically. In other words, according to the buckling definition, plasticity in the first category columns does not appear before they display significant bending vibration, while in the second category columns the case is reversed. The two inequalities also indicate that the load-carrying capacity of the slammed columns depends on the dynamic post-buckling elasto-plastic behavior.

An interesting phenomenon is found from the present experiments: when a column is slammed in the vicinity of $\varepsilon_{c,crf}$, its slamming pulse shape changes in contrast with the previous one. In particular, the shape is completely distorted while the plastic failure occurs. This phenomenon is displayed in Fig. 12 where the pulse shape is essentially a semi-sine wave before the plastic failure appearance but it is twisted out of the original shape at and beyond the collapse slamming. The phenomenon is related to the development of plastic deformation in a slammed column. It is known that the plastic region of a slammed column appears first at the two sides of the center and then develops along the axial length and over the cross-section thickness; thereby the flexural rigidity in the middle part diminishes gradually with the decrease of the corresponding elastic region. When the plastic region spreads to such an extent that the plastic rigidity overwhelmingly prevails in dominating the total middle-length flexural rigidity, the middle part of the column behaves similarly as a plastic spring while the two side parts behave like rigid rods. Thus, there is a sharp transformation from the elasto-plastic column to a system made of two rigid rods and a plastic spring. Correspondingly, between the water surface and the slamming unit, a sudden change occurs from fluid -"hard structure" slamming to fluid -"soft structure" slamming. As a result, it seems that the whole slamming process consists of two sub-slamming ones which have the two different striking bodies. The "rigid rod–plastic spring" model is corroborated by Fig. 13 in which the axial compressive strain distribution of S11 at the collapse slamming is indicated, and the plastic hinge is marked by the near zero value at the center.

The residual plastic collapse patterns for the specimens of S11–S15 are shown in Fig.
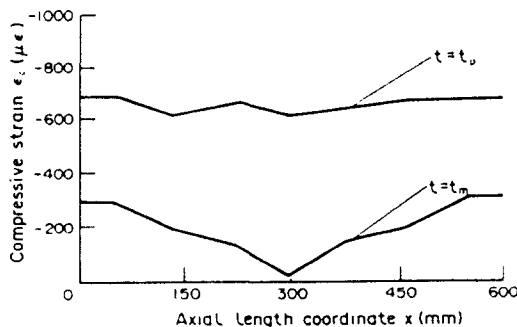

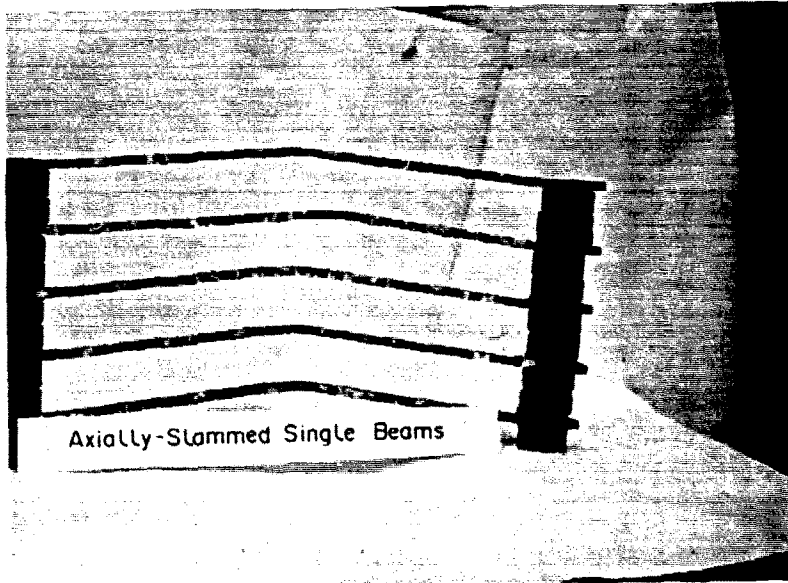Fig. 13. Compressive strain distribution at collapse slamming (specimen no. S11).

Fig. 14. Residual plastic collapse patterns.

14. It is evident that the middle part of the specimens is curved and the two side parts are straight. This further verifies that under collapse impact the elasto–plastic columns become a "rigid rod–plastic spring" system.

(5) Loading sequence effect

As mentioned in previous sections, in order to obtain the plastic collapse critical loading values in Table 1, several tests are performed for a column with ε_c greater than the yield strain ε_y. Since this involves testing damaged columns, the effects of the loading sequence before collapse on the critical strain $\varepsilon_{c,cr}$ should be considered. Table 4 gives the loading histories of several tested columns in the form of a sequence of peak ε_c in which the values in the brackets represent the maximum resultant strains at the corresponding ε_c. These listed sequences are between the first elasto-plastic loading (before which the column's response is elastic) and the collapse loading. Two observations are to be made from Table 4: (1) $\varepsilon_{c,cr}$ is insensitive to the loading sequences and has almost the same values for each of the columns with the same length; (2) the maximum resultant strains at and beyond $\varepsilon_{c,cr}$ strongly depend on the test histories.

In order to indicate the dependence of $\varepsilon_{c,cr}$ on the column's post-buckling elasto-plastic behavior in one slamming, the plastic region distribution for S11 at $\varepsilon_c = 600$ and $\varepsilon_c = 680$ and for S13 at $\varepsilon_c = 650$ and $\varepsilon_c = 500$ are given in Figs 15 and 16, respectively. From Fig. 15, it is seen that at the $\varepsilon_c = 600$ slamming the elastic region prevails in the column's middle part since the larger plastic region appears only at the compressive side, and the plasticity at the tensile side is negligible. This makes it natural that elasticity dominates the column's response at the present slamming; therefore, the column still behaves in an elastic way. At the next impact ($\varepsilon_c = 680$), the dominant plastic region is formed in the middle part, and plasticity controls the column's behavior. This leads the structure to a critical collapse condition, and the subsequent slamming results in decreases in the peak loading magnitude and increases in the plastic strain. For S13, the case is different from that of S11. Since at the $\varepsilon_c = 650$ slamming (the first elasto-plastic loading) the dominant plastic region is produced and plasticity dominates the column's behavior, the present impact has led the

Table 4. Specimen loading sequences between ε_y and $\varepsilon_{c,cr}$

Specimen no.	Loading sequences ε_c ($\mu\varepsilon$)						$\varepsilon_{c,cr}$ ($\mu\varepsilon$)
S11	600 (1868)	680 (2668)	450 (8150)				680
S12	570 (1334)	680 (1934)	669 (2335)	550 (2935)			680
S13	650 (2730)	500 (3308)					650
S21	640 (1615)	693 (2230)	720 (2384)	775 (2846)	800 (7600)	417 (18000)	800
S22	567 (1358)	662 (1923)	672 (2145)	786 (5538)	602 (8538)		780
S23	790 (3608)	506 (8050)					790
S31	913 (2101)	913 (2600)	913 (5800)	700 (15180)			900
S32	652 (1334)	870 (2001)	930 (6600)	869 (10887)			910
S33	650 (1334)	869 (2268)	946 (6750)	780 (9768)			930
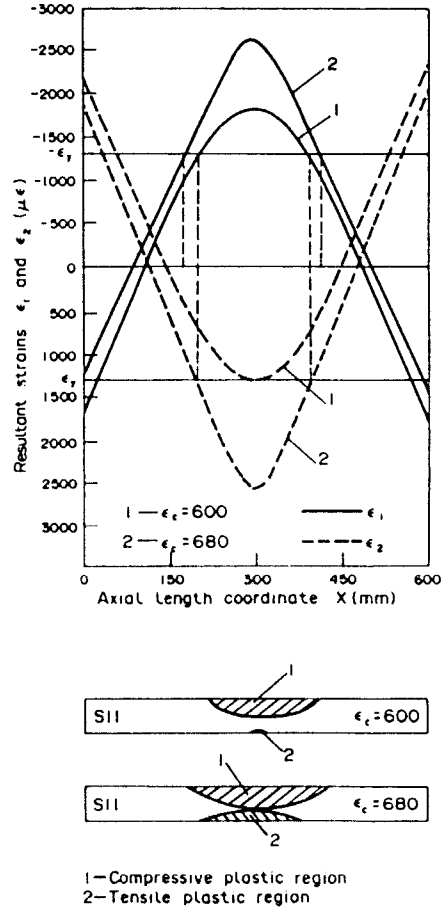
Fig. 15. Determination of plastic regions at t_M (specimen no. S11).
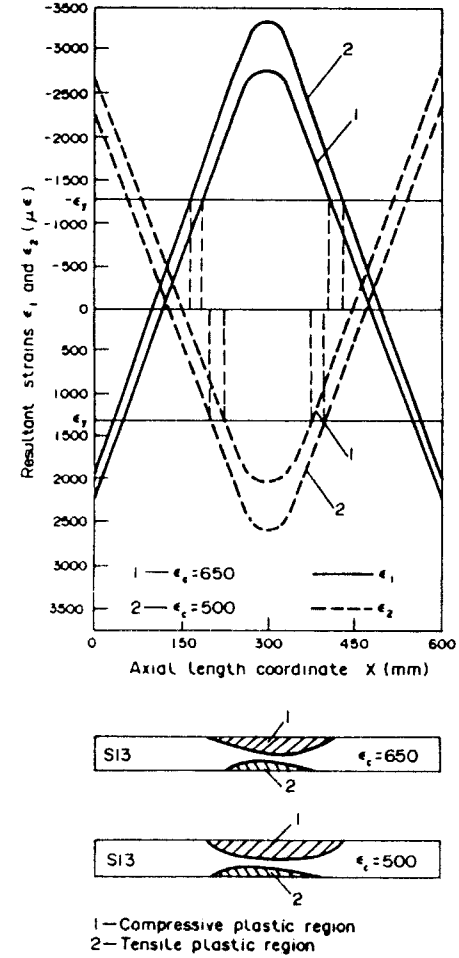
Fig. 16. Determination of plastic regions at t_M (specimen no. S13).

structure to the critical failure state and the next slamming results in the decreasing peak loading value ($\varepsilon_c = 500$) and the increasing plastic strain. However, the two different cases for S11 and S13 bring about almost identical $\varepsilon_{c,crf}$ values. Similar situations are found for the other tested columns. Consequently, it is concluded that the load-carrying capacity of an axially-slammed column is insensitive to the elasto-plastic loading histories which the structure experiences before $\varepsilon_{c,crf}$, and is essentially governed by the dynamic post-buckling elasto-plastic behavior in one slamming.

CONCLUSIONS

This paper describes results from experiments in which each of 15 columns is loaded by attaching its upper end to a mass and lower end to a splash plate, and then dropped the unit into water from a series of heights. The essential results are given in Table 1.

For impact loads less than collapse values, the axial compression pulses are essentially semi-sine waves with durations ranging from 15 to 24 msec. At these durations, from 130 to 311 wave transits occur along column lengths of 400–600 mm in the tests. Thus, loading may be considered to be axially uniform. Also, at critical loading magnitudes, these load durations are sufficiently long for the response to be dominated by motion in the fundamental mode. For each column, three critical conditions are observed in the experiments: plastic incipience, buckling and plastic collapse. These conditions are estimated by introducing three critical peak axial loading strains which are the critical buckling peak axial loading strain $\varepsilon_{c,crb}$, the critical plastic peak axial loading strain $\varepsilon_{c,cry}$ and the critical collapse peak axial loading strain $\varepsilon_{c,crf}$.

For each column, the three critical loading values are reported. The results indicate that: (1) the plasticity in a column appears first at the center and the plastic region is always at the middle length; (2) according to the buckling definition, the type 1 columns buckle elastically while the type 2 columns buckle plastically; and (3) the columns' load-carrying capacity is insensitive to the elasto-plastic loading histories (sequences) before the plastic collapse occurs and is essentially governed by the dynamic post-buckling elasto-plastic behavior in one slamming.

REFERENCES

Abrahamson, G. R. and Goodier, J. N. (1966). Dynamic flexural buckling of rods with a plastic compression wave. *J. Appl. Mech.* **33**, 241–247.
Ari-Gur, J., Weller, T. and Signer, J. (1982). Experimental and theoretical studies of columns under axial impact. *Int. J. Solids Structures* **18**, 619–641.
Bolotin, V. V. (1964). *The Dynamic Stability of Elastic Systems*. Holden-Day, San Francisco.
Grybos, R. (1973). Impact stability of a bar. *Int. J. Engng Sci.* **13**, 463–478.
Hayashi, T. and Sano, Y. (1972). Dynamic buckling of elastic bars (1st report). *Bull. JSME* **15**, 1167–1175.
Hayashi, T. and Sano, Y. (1973). Dynamic buckling of elastic bars (2nd report). *Bull. JSME* **15**, 1176–1184.
Housner, G. N. and Tso, W. K. (1962). Dynamic behavior of supercritically loaded struts. *J. Engng Mech. Div.* **88**, 41–65.
Jonse, N. and Dos Reis, H. L. M. (1980). On the dynamic buckling of a simple elastic-plastic model. *Int. J. Solids Structures* **16**, 969–989.
Koji Fukatsu, Koichiro Kawashima and Masanobu Oda (1986). The dynamic elastic-plastic buckling of bars with initial deflection. *Trans. JSME* **52**, 2311–2318.
Koji Fukatsu, Koichiro Kawashima and Masanobu Oda (1987). The dynamic elastic-plastic buckling of bars with initially curved bars. *Int. J. Plast.* **3**, 149–156.
Kunistomo Sugiura, Eiji Mizuno and Yuhshi Fukumoto (1985). Dynamic instability analysis of axially impacted columns. *J. Engng Mech.* **111**, 893–908.
Lee, L. H. N. (1981). Dynamic buckling of an inelastic column. *Int. J. Solids Structures* **17**, 271–279.
Lindberg, H. E. (1965). Impact buckling of a thin bar. *J. Appl. Mech.* **32**.
Lindberg, H. E. and Florence, A. L. (1987). *Dynamic Pulse Buckling—Theory and Experiment*. Kluwer, The Netherlands.
Reiss, E. L. and Matkowsky, B. J. (1971). Nonlinear dynamic buckling of a compressed elastic column. *Q. J. Appl. Math.* **29**, 245–260.
Simitses, G. J. (1987). Instability of dynamically-loaded structures. *Appl. Mech. Rev.* **40**, 1403–1408.
Taub, J. and Kong, V. C. (1934). Impact buckling of thin bars in the elastic range hinged at both ends. NACA, TM748.